



Machine learning-based multipath modeling in spatial domain applied to GNSS short baseline processing

Yuanxin Pan¹ · Gregor Möller^{1,2} · Benedikt Soja¹

Received: 6 February 2023 / Accepted: 25 September 2023 / Published online: 16 October 2023
© The Author(s) 2023

Abstract

Multipath is the main unmodeled error source hindering high-precision Global Navigation Satellite System data processing. Conventional multipath mitigation methods, such as sidereal filtering (SF) and multipath hemispherical map (MHM), have certain disadvantages: They are either not easy to use or not effective enough for multipath mitigation. In this study, we propose a machine learning (ML)-based multipath mitigation method. Multipath modeling was formulated as a regression task, and the multipath errors were fitted with respect to azimuth and elevation in the spatial domain. We collected 30 days of 1 Hz GPS data to validate the proposed method. In total, five short baselines were formed and multipath errors were extracted from the postfit residuals. ML-based multipath models, as well as observation-domain SF and MHM models, were constructed using 5 days of residuals before the target day and later applied for multipath correction. It was found that the XGBoost (XGB) method outperformed SF and MHM. It achieved the highest residual reduction rates, which were 24.9%, 36.2%, 25.5% and 20.4% for GPS P1, P2, L1 and L2 observations, respectively. After applying the XGB-based multipath corrections, kinematic positioning precisions of 1.6 mm, 1.9 mm and 4.5 mm could be achieved in east, north and up components, respectively, corresponding to 20.0%, 17.4% and 16.7% improvements compared to the original solutions. The effectiveness of the ML-based multipath model was further validated using 30 s sampling data and data from a low-cost device. We conclude that the ML-based multipath mitigation method is effective, easy to use, and can be easily extended by adding auxiliary input features, such as signal-to-noise ratio, during model training.

Keywords GNSS · Multipath · Spatial domain · Machine learning · XGBoost

Introduction

Global Navigation Satellite System (GNSS) has already become an essential part of our daily life and a crucial part of the geodetic infrastructure (Rebischung et al. 2016). With the refinement of error correction models and the improvement of precise products provided by the International GNSS Service (IGS), GNSS-based positioning precision can reach mm-level in static mode and cm-level in kinematic mode (Bock et al. 2004; Choy et al. 2016). However, multipath still remains the main unmodeled error source due to its nonlinear nature. It degrades the contribution of GNSS to

applications demanding high precision, such as earthquake early warnings (Larson 2009).

Multipath is the effect of simultaneous reception of direct and reflected GNSS signals. It is almost inevitable due to the nondirectional nature of GNSS antennas. Apart from choosing a less reflective environment, hardware- and software-based measures are usually adopted to reduce multipath. The hardware-based methods, such as choke ring, can only reduce part of the multipath error (Park et al. 2004). The software-based approaches include various filtering methods utilizing the frequency signature of multipath (Satirapod and Rizos 2005). However, it is hard to apply such filtering when the multipath frequency range overlaps with that of signals of interest. Signal-to-noise ratio (SNR) measured by GNSS receivers can be used for multipath characterization or observation weighting (Bilich et al. 2008; Su et al. 2021). However, its efficiency is dependent on the SNR data quality and antenna gain pattern. Sidereal filtering (SF) is a widely used method to mitigate multipath for high-precision GNSS

✉ Yuanxin Pan
yxpan@ethz.ch

¹ Institute of Geodesy and Photogrammetry, ETH Zurich, 8093 Zurich, Switzerland

² Present Address: Department of Geodesy and Geoinformation, TU Wien, 1040 Vienna, Austria

data processing (Genrich and Bock 1992). The idea is that the geometric relation between the Global Positioning System (GPS) constellation and a static station will repeat every sidereal day, and the positioning error induced by multipath will also repeat after the same period. Hence, the coordinate time series of previous days, with proper time shifts, can be used to correct the multipath for the target day. The key to implement SF is to calculate the correct orbit repeat period for each satellite, since the actual orbit repeat period of GPS is not exactly one sidereal day and even varies with different satellites (Choi et al. 2004; Agnew and Larson 2006). When it comes to multi-GNSS, the case is more complicated and SF can no longer be applied in the coordinate-domain. In order to solve this problem, observation-domain SF was first proposed by Zhong et al. (2010) for baseline processing and was also successfully applied to precise point positioning (PPP) and multi-GNSS processing (Atkins and Ziebart 2015; Ye et al. 2014; Geng et al. 2018). It extracts multipath corrections from postfit residuals of previous days and applies them to the observations of each satellite on the target day after shifting the corrections by individual orbit repeat periods. This process is not easy to implement, particularly considering the varying repeat periods for different satellites and days (Choi et al. 2004). Furthermore, its effectiveness for multipath mitigation can sometimes be affected by orbital maneuvers.

The spatiotemporal repeatability of multipath can also be modeled in the spatial domain. It is based on the fact that multipath errors mainly depend on satellite positions in a skyplot, and thus a multipath correction model can be established with respect to azimuth and elevation angles in a topocentric coordinate system. Dong et al. (2015) named this kind of spatial domain-based multipath model as multipath hemispherical map (MHM) and compared its performance with SF using 1 Hz GPS data from a dual-antenna receiver. It was concluded that similar multipath mitigation performance could be achieved with both methods, but MHM was less effective for high-frequency multipath. However, MHM is satellite independent and is easy to implement and use (Zheng et al. 2019). Wang et al. (2019) modified the MHM method by introducing a set of trend surface coefficients for each grid to capture the multipath variation within a grid. It was found that the modified MHM method achieved about 5% more residual reduction rate than MHM, but it complicated the implementation of the original MHM method.

Over the last decade, artificial intelligence, especially machine learning (ML), has become more and more prominent in geosciences (Li et al. 2011; Beroza et al. 2021). Such data-driven algorithms are suitable for solving nonlinear problems, including classification and regression tasks. ML algorithms have already been applied to GNSS multipath and non-line-of-sight (NLOS) signal classification (Hsu 2017). Suzuki et al. (2020) trained a convolutional neural network (CNN) to detect

NLOS signals based on the output of multiple GNSS signal correlators of a software-defined receiver and reported a 98% classification accuracy. Tao et al. (2021a, b) used neural networks to mine the multipath features in coordinate and frequency domains, respectively, and reported better multipath mitigation performance than conventional methods. However, currently there is no research that studies the possibility of multipath modeling in the spatial domain with ML.

This research focuses on investigating the potential of ML algorithms on multipath modeling in the spatial domain. We formulate multipath modeling as a regression task for ML algorithms. The multipath errors are fitted with respect to azimuth and elevation angles in the skyplot. The benefit of SNR measurements for multipath modeling is also examined. Three widely used ML methods, i.e., random forest (RF), extreme gradient boosting (XGB) and multilayer perceptron (MLP), are tested regarding multipath mitigation for short baselines. The principles of multipath modeling are introduced in next section. Then, the data used in this study are described, and the ML-based multipath mitigation results are displayed and discussed. Finally, conclusions and outlooks are given.

Multipath modeling

Multipath cannot be modeled thoroughly due to its nonlinearity. But under the assumption of specular reflection, the multipath errors of pseudorange and carrier phase can be modeled as (Bilich et al. 2007):

$$\begin{cases} P_{MP} = \frac{\alpha \cdot \delta \cdot \cos \varphi}{1 + \alpha \cos \varphi} \\ \Phi_{MP} = \tan^{-1} \frac{\alpha \sin \varphi}{1 + \alpha \cos \varphi} \end{cases} \quad (1)$$

where P_{MP} and Φ_{MP} are multipath errors of pseudorange and carrier phase, respectively. We denote the reflection coefficient as α , which is the amplitude ratio between the reflected signal and the direct signal. The geometric path delay is denoted as δ , and φ is the phase offset of the reflected signal, which is caused by the extra path delay and phase shift due to the reflection.

The SNR measured by a receiver is a useful indicator of multipath errors. It contains the reflection information of the environment:

$$\text{SNR}^2 = A_d^2 + A_m^2 + 2A_d A_m \cos \varphi \quad (2)$$

where A_d and A_m are the amplitudes of direct and reflected GNSS signals. The symbol φ has the same meaning as in Eq. (1). It can be noted that φ is the common underlying parameter for multipath and SNR, which means that SNR measurements could be beneficial for multipath modeling.

ML-based multipath modeling

ML algorithms have been proven to be powerful tools for regression tasks. The main advantage of ML over classic spatial interpolation algorithms is that not only azimuth and elevation angles but also auxiliary information, such as SNR measurements, can be utilized for interpolation. There are a lot of ML algorithms suitable for regression tasks. Among them, ensemble learning algorithms, including bagging and boosting, are usually ranked among the best-performing methods. Besides, artificial neural networks (ANN) are also commonly used ML algorithms. Hence, three representative ML algorithms, including random forest (RF), extreme gradient boosting (XGB) and multilayer perceptron (MLP), are selected as the candidate methods for multipath modeling in this study. RF is an ensemble learning method that outputs the average results of a set of randomized decision trees (Breiman 2001). It can overcome the overfitting issue of a single decision tree and usually can achieve high accuracy without complex configuration. XGB is an open-sourced gradient boosting framework (Chen and Guestrin 2016). The basic idea is that a set of decision trees are trained sequentially to better fit the samples with larger residuals, and it is widely used due to its high performance. MLP is a type of ANN with fully connected nodes. It consists of three parts, i.e., input layer, hidden layer(s) and output layer. Nonlinear activation functions are used at each node, and thus can simulate the nonlinear relation between input and output.

Data preparation is the key to ML model training. Two sets of data, i.e., input features and a target vector need to be provided. Apart from azimuth and elevation, SNR is also tested as an additional input feature in this study. The target vector is an array of multipath errors, which are the denoised single-differenced (SD) residuals extracted from double-differenced (DD) residuals during baseline processing. The detailed multipath extraction method is described by Ye et al. (2014). Note that a low-pass filter with an empirical corner frequency of 0.1 Hz is used to denoise the SD residuals in this study (Choi et al. 2004; Geng et al. 2018). It is usually recommended to stack 5–7 days' residuals to build the multipath model for improved performance (Dong et al. 2015; Wang et al. 2019). Finally, ML models are trained to best fit the relation between input features and the target vector. Note that all the training data should be cleaned for outliers and normalized to improve training stability and model performance. The basic procedures of GPS data processing and ML-based multipath mitigation are illustrated in Fig. 1. Note that daily updating of the ML model is not necessary and is only adopted if the optimal model performance is desired. In other words, the model has the capability to

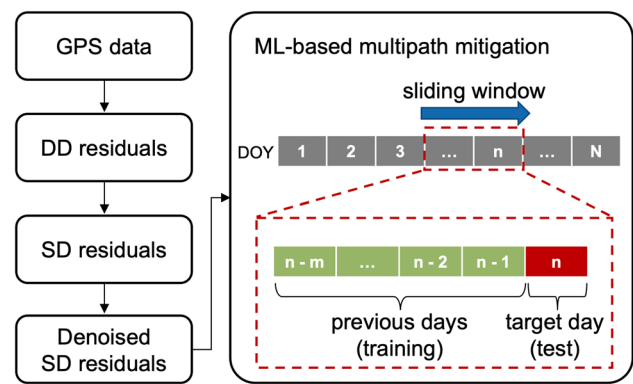


Fig. 1 Flowchart of GPS data processing and ML-based multipath mitigation. The ML model is trained using the data from previous days, and it predicts the multipath errors for the target day

predict multipath for multiple days, but this comes with a performance trade-off. More details about optimal ML model construction can be found in the Results section.

Data

We obtained 30 days (DOY 244–273 of 2021) of 1 Hz high-rate GPS data from Curtin University to test the ML-based multipath mitigation method. There were four GPS antennas on the rooftop of Curtin University (Fig. 2). The antenna connected to a Trimble NetR9 receiver (CUTO) was used as the reference station. The other three antennas were all connected to two different receivers, forming six rover stations, i.e., CUA/CUTA, CUBB/CUTB and CUCC/CUTC (see details in Table 1). Here, a station denotes the combination of an antenna and a receiver. Station CUBB was excluded in the following studies since there were many gaps in its data. Hence, five short baselines were formed between CUTO and rover stations for multipath mitigation experiments. The baselines were processed with a modified version of the RTKLIB software (Takasu 2009). Uncombined observations of pseudorange and carrier phase on dual frequencies were utilized for parameter estimation. An elevation cut-off angle of 10° was adopted, and no SNR mask was applied. Since the distance between the reference station and any rover station was less than 10 m, tropospheric and ionosphere delays were eliminated by differencing between stations. Only rover positions and DD ambiguities were estimated in a Kalman filter. Specifically, rover positions were estimated in static mode to obtain postfit residuals including multipath and noise. It was worth noting that all the stations had the same type of antenna (Table 1), which meant antenna PCV (Phase Center Variation) errors could be eliminated through differencing and would not affect multipath modeling. Finally, multipath errors were extracted from the

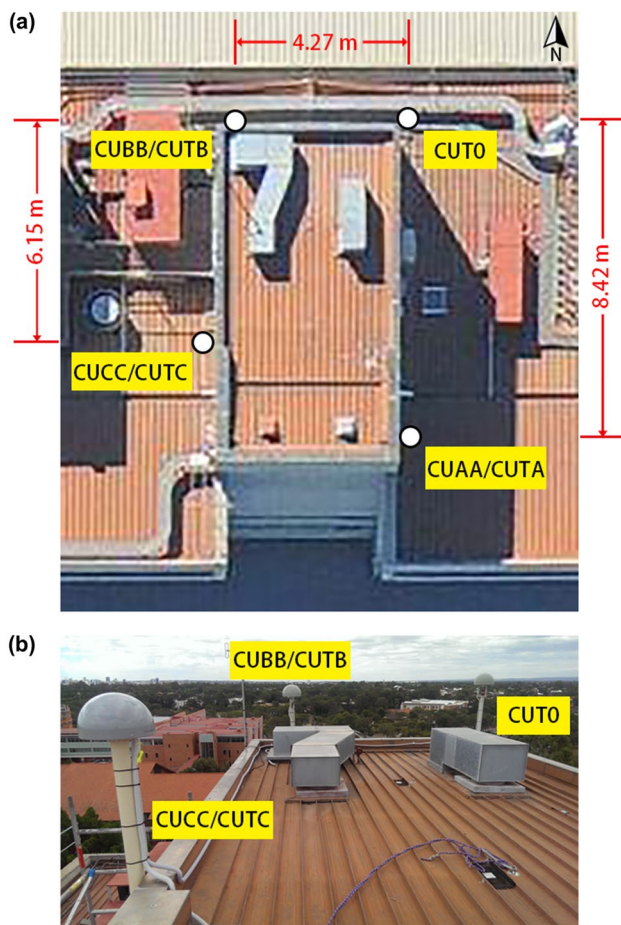


Fig. 2 Distribution of GPS stations and the observation environment on the rooftop of Curtin University. CUTO is the reference station used for relative positioning. All three rover antennas are connected to two different receivers, respectively. (a) Bird's-eye view (b) South view. The copyright of the photos is preserved by Curtin GNSS-SPAN Group

postfit residuals (Ye et al. 2014) and were used for multipath modeling in the following experiments. The observation-domain SF and MHM multipath models were built on the same data set for comparison. Note that observation-domain SF is simply denoted as SF in the remaining text for clarity.

The orbit repeat period required by SF was calculated using broadcast ephemerides for each satellite (Choi et al. 2004), and the MHM model was constructed with 1° by 1° grids for improved model stability and effectiveness (Dong et al. 2015). Multipath models for GPS P1, P2, L1 and L2 observations were constructed individually.

Results

We first analyze the characteristics of the extracted multipath errors. Then, different input features and ML algorithms are explored to establish the multipath models. Finally, the ML-based multipath mitigation method is compared to the conventional observation-domain SF and MHM methods regarding residual reduction and positioning improvement. Considering the similar data quality and multipath environment, we take the station CUCC as the example for specific analysis and present the statistical results for all the stations.

Multipath characteristics analysis

The key to set up a reliable multipath model is the spatiotemporal repeatability of multipath. Figure 3 shows the low-pass filtered residuals of satellite G04 at CUCC station on DOY 244, 245 and 249. The Pearson correlation coefficients between DOY 244 and 249 can reach 0.68, 0.70, 0.82 and 0.86 for P1, P2, L1 and L2, respectively. It indicates that the environment around the stations is stable during the experiment periods. Considering the good temporal correlation, we stacked 5 days of residuals before the target day to enhance the multipath signals during modeling (Dong et al. 2015). We also checked the multipath correlation between both frequencies for pseudorange and carrier phase, respectively. The correlation coefficients between P1 and P2 residuals are below 0.2 and most of the time close to 0. This indicates that the multipath errors of different pseudorange measurements are not correlated. For carrier phase residuals on dual-frequency, the correlation coefficients vary between 0 and 0.5. Hence, there is no definite relation between L1 and L2 multipath effects. Considering the same path delay but

Table 1 Detailed configurations of GPS stations used in this study

Station	Receiver type	Firmware version	Antenna type
CUTO	Trimble NetR9	5.45	TRM59800.00 SCIS (Choke ring antenna)
CUTA		5.22	
CUTB		5.22	
CUTC		5.45	
CUAA	Javad TRE_G3T DELTA	3.7.9	
CUBB			
CUCC			

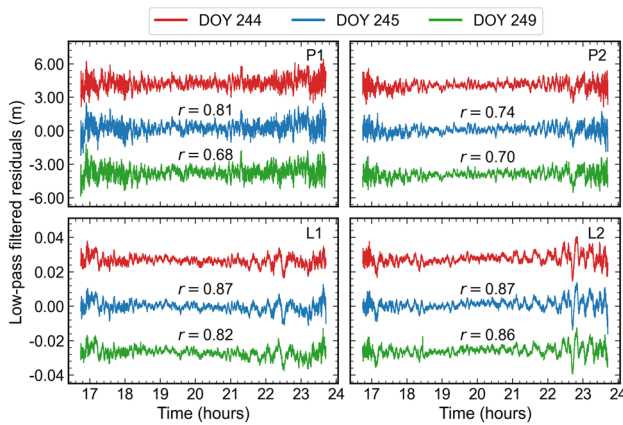


Fig. 3 Low-pass filtered residuals of satellite G04 at station CUCC. Pseudorange and carrier phase residuals are shown in the upper and bottom panels, respectively. Residuals on DOY 244, 245 and 249 are denoted by red, blue and green curves, respectively, and they are shifted by corresponding orbit repeat periods along the x-axis to better show the temporal correlation. Shifts along the y-axis are made to avoid overlapping. Pearson correlation coefficients with respect to the residuals of DOY 244 are denoted above each curve for DOY 245 and 249

different wavelengths of L1 and L2 carriers, the phase of the two reflected carriers is usually unsynchronized, and thus the disturbance on the direct carrier signals will be different and uncorrelated (Bilich et al. 2007).

Optimal ML-based multipath model setup

To select the best ML algorithms and input feature combinations, we used 30 days of data from the CUCC station to evaluate the performance of each combination regarding the residual reduction rate. The three candidate ML algorithms included RF, XGB and MLP, and the potential input features included azimuth, elevation and SNR. Note that while multipath combination is a direct metric for pseudorange multipath variation (Hilla and Cline 2004), based on our initial test, it does not enhance carrier phase multipath modeling due to the different multipath characteristics between pseudorange and carrier phase (Bilich et al. 2007). Thus, it is not considered as a candidate feature. Since azimuth and elevation were necessary for spatial interpolation, there were only two choices for input features, i.e., with or without SNR. In this study, we employed calibrated SNR instead of raw SNR measurements extracted from RINEX (Receiver Independent Exchange Format) files. The reason for this choice is that variations in raw SNR are not solely caused by multipath effects but are also influenced by satellite elevation (Strode and Groves 2016). To remove the elevation impact, a polynomial of degree 3 was fitted to raw SNR as a function of elevation, and it was then used to calibrate the raw SNR measurements (Lyu and Gao 2020a, b; Strode and Groves

Table 2 Optimal set of hyperparameters derived from the grid search

Algorithm	Hyperparameter	Value
RF	n_estimators	10
	Max_depth	30
	Criterion	Squared_error
XGB	n_estimators	40
	Max_depth	20
	Criterion	Squared_error
MLP	Hidden_layer_sizes	(128, 128, 128, 128, 128, 128)
	Activation	Relu
	Solver	Adam

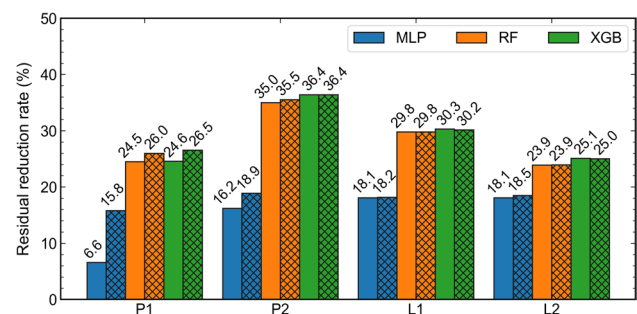


Fig. 4 Mean residual reduction rates for station CUCC over DOY 250–273. The reduction rates using MLP, RF and XGB (only azimuth and elevation as input features) are denoted by blue, orange and green bars, respectively. The shaded bars represent the corresponding models with calibrated SNR as an additional input feature

2016). ML-based multipath models with the six possible combinations of algorithms and input features were trained on the residuals of DOY 244–248 and validated using the residuals of DOY 249, respectively. Grid search was adopted for hyperparameter tuning. The optimal hyperparameters (Table 2) were determined based on the residual reduction rates for DOY 249. Note that adding calibrated SNR as an additional input feature had little impact on the optimal hyperparameters for each ML algorithm according to our experiments. After determining the best hyperparameters, model training and testing were repeated for the remaining 24 days (see Fig. 1), and mean multipath reduction rates were calculated for each combination.

Figure 4 shows the average residual reduction rates for all six combinations. It indicates that including calibrated SNR as an additional feature does not improve model performance for carrier phase multipath mitigation, especially for RF and XGB. It even adversely affects carrier phase multipath mitigation for some days. Still, adding SNR can slightly improve the model performance for pseudorange multipath mitigation, especially for MLP. The primary reason is that

theoretically, SNR and pseudorange multipath are in phase, but there is a time lag between SNR variation and carrier phase multipath (Strode and Groves 2016; Zhang et al 2019). However, this time lag varies with different multipath signals, and it needs further studies on how to better utilize SNR to improve carrier phase multipath modeling. Another reason may be that the numerical precision of SNR values in the RINEX files is not high enough. The Trimble and Javad receivers involved in this study only record SNR measurements with a precision of 0.2 dB-Hz and 0.25 dB-Hz, respectively. Such coarse SNR increments are not precise enough to improve multipath modeling. Bilich et al. (2007) also found this issue and reported that it was receiver model dependent. Using only azimuth and elevation angles as input features are sufficient for RF and XGB models. Residual reduction rates of 25%, 36%, 30% and 25% can be achieved for P1, P2, L1 and L2, respectively. SNR is excluded as a feature to prevent any potential deterioration in carrier phase multipath modeling. It is worth pointing out that although RF can conduct multivariate regression (i.e., one multipath model for four observables), no obvious improvement can be observed compared to the results of building multipath models individually. Since XGB with azimuth and elevation as input features can achieve highest residual reduction rates, we only present the results of this combination for ML-based methods in the following experiments.

Multipath mitigation test

After picking the optimal ML algorithm and input features, we tested and compared the multipath mitigation performance for three different methods: SF, MHM and XGB.

Multipath model

The multipath models based on the XGB method are visualized in Fig. 5 for station CUCC on DOY 251. It can be seen that most severe multipath errors concentrate in the low-elevation areas, and there is no obvious pattern difference with respect to azimuth. This is because there is no strong reflection source around the station, and most reflected signals come from the surrounding grounds (Fig. 2). Such an observation environment is similar to most IGS stations and can make the conclusions of this study generally applicable. We further plotted the multipath correction time series of SF, MHM and XGB in Fig. 6a to directly compare their capability of modeling multipath. The corresponding low-pass filtered residuals of satellite G10 are also included as the reference. It can be found that the multipath models of SF and XGB are in good agreement with the low-pass filtered residuals for both pseudorange and carrier phase on dual frequencies. They successfully replicate both the long- and short-term variations induced by multipath. However,

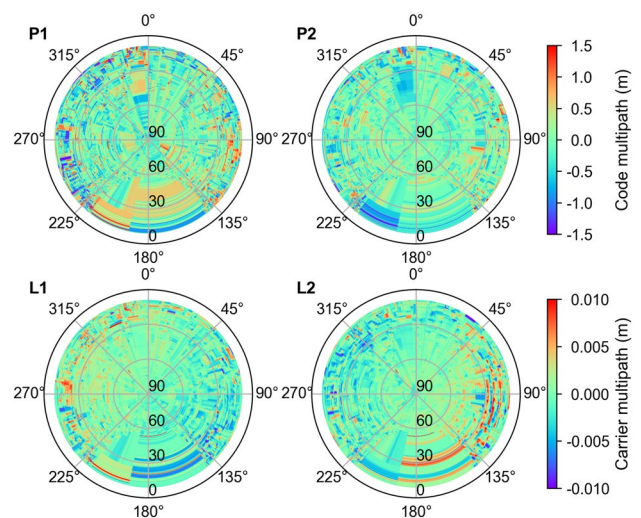


Fig. 5 Visualization of XGB-based multipath models for station CUCC on DOY 251

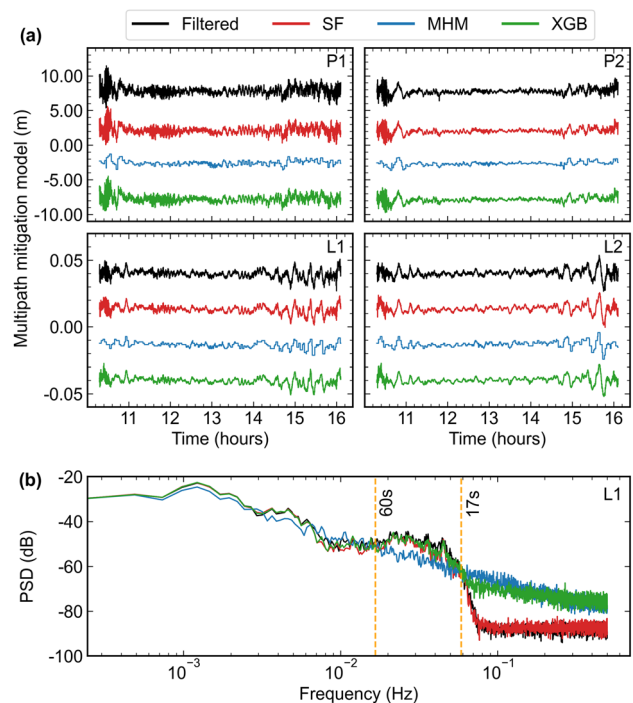


Fig. 6 Low-pass filtered residuals and different multipath models for satellite G10 at station CUCC on DOY 251 and the corresponding PSDs for L1. **a** The filtered residuals and multipath models of SF, MHM and XGB are displayed in black, red, blue and green, respectively. The individual curves are shifted vertically to avoid overlapping. **b** L1 PSDs (relative to 1 m²/Hz) for low-pass filtered residuals and different multipath models. The two orange vertical lines represent the frequency range from 17 to 60 s

MHM can only capture the long-term tendency but not the short-term changes, i.e., high-frequency components. This

drawback is most obvious during the period from 14 to 16 h when the satellite is at low elevation and multipath changes fast. The MHM multipath model in this period resembles a low-resolution version of SF and XGB models.

Figure 6b exhibits the power spectral density (PSD) for L1 multipath models generated by three methods as well as the low-pass filtered residuals. The MHM model has a lower power density between the frequency range from 17 to 60 s. Compared to XGB, MHM is about 7 dB lower for the high-frequency multipath components, which accounts for around 80.5% lower signal power. This explains the low resolution of the MHM model in Fig. 6a. For lower frequencies, MHM agrees well with the other two methods. In contrast, the PSDs of SF and XGB are in good agreement with that of low-pass filtered residuals from 17 s to the lowest frequency. The PSD drop before 0.1 Hz of the SF model and the low-pass filtered residuals is caused by the low-pass filter used to remove the white noise in raw residuals. The higher noise level in the XGB model between 2 and 17 s is most probably caused by spatial interpolation errors, but it does not affect the multipath mitigation effect since the noise magnitude is very small compared to multipath errors. A similar phenomenon is also observed for MHM, although it is not expected since the MHM model averages the residuals within each grid and the noise level should be lower. Hence, the higher noise level is possibly an artifact caused by the step signals generated by the low-resolution MHM model as shown in Fig. 6a. Overall, the PSD analysis confirms that the ML-based multipath model can achieve similar performance as SF and outperforms the MHM model due to the advantage of spatial interpolation.

Residual reduction

Figure 7 shows the posterior residuals of G10 at station CUCC on DOY 251 and those corrected using SF, MHM and XGB methods. The multipath errors are effectively reduced by all three methods, especially for periods when the satellite is at low elevations. The RMS of the residuals corrected with XGB is the smallest among the three methods, reaching 0.55 m, 0.27 m, 2.25 mm and 2.52 mm for P1, P2, L1 and L2, respectively. Compared to the raw residuals, the improvements are 26.7%, 41.3%, 36.6% and 30.6%, respectively. Here, it can be found that the reduction rate for P1 is much smaller than for P2. This can be explained by the higher noise level of P1 residuals. The multipath mitigation performance of SF is similar to that of XGB, and the RMS differences between them are only 0.01 m, 0.01 m, 0.00 mm and 0.02 mm for P1, P2, L1 and L2, respectively. This is reasonable as observation-domain SF represents the state-of-the-art method for establishing multipath models and multipath alignment error is within 1 s if the orbit repeat period for each satellite is accurately obtained. In contrast,

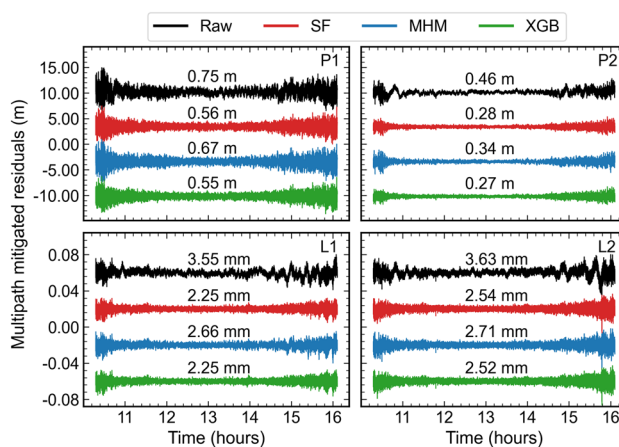


Fig. 7 Raw and multipath corrected residuals of satellite G10 at station CUCC on DOY 251. The raw residuals and those corrected with SF, MHM and XGB are represented by black, red, blue and green curves, respectively. The individual curves are shifted along the y-axis to avoid overlapping. The RMS value is denoted above each curve

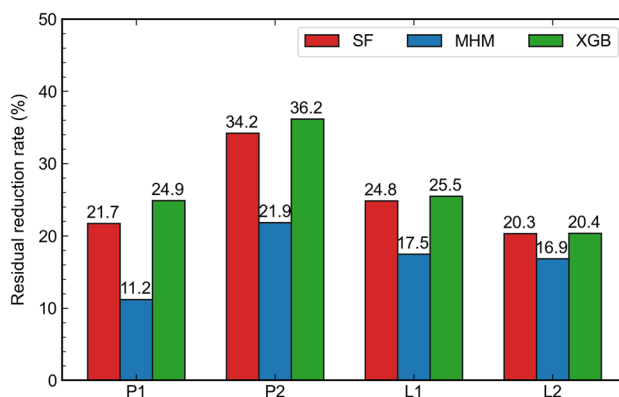


Fig. 8 Mean residual reduction rates using different multipath mitigation methods over all five stations and 25 days

MHM can only achieve improvements of 10.6%, 26.1%, 25.1% and 25.3% for the four observables. That is because MHM cannot effectively capture the high-frequency multipath components. This can be seen in the L1 residual time series between 14 and 16 h in Fig. 7. There are still obvious fluctuations in this period after being corrected with MHM, especially the variations near 15 h. Such fluctuations nearly disappear when XGB or SF models are applied.

The mean residual reduction rates using SF, MHM and XGB over all five stations and 25 days are displayed in Fig. 8. Overall, the results are consistent with those shown in Fig. 7, i.e., XGB performs similarly to SF and better than MHM regarding residual reduction rates. After multipath mitigated with XGB, RMS improvements of 24.9%, 36.2%, 25.5% and 20.4% can be achieved for P1, P2, L1 and L2 residuals, respectively. The reduction is 0.1% to 0.7% and

2.0% to 2.8% larger than for SF for carrier phase and pseudorange residuals, respectively. In contrast, the reduction rates achieved with MHM are 13.7%, 14.3%, 8.0% and 3.5% less than for XGB for P1, P2, L1 and L2, respectively, due to its deficiency of modeling high-frequency multipath signals.

Thus far, we have always used the residuals of the latest 5 days before the target day to set up the multipath model. Although the best correction effect can be obtained this way, updating the model daily is cumbersome. It would be beneficial, especially for real-time applications, if the multipath model can be applied to subsequent days without too much precision loss. Hence, we tested the model validity period for all five stations and compared the performance among SF, MHM and XGB. Residuals from DOY 244–248 are used to set up the multipath model, and later, it is applied for multipath correction on days from DOY 249 to 273. The mean residual reduction rates over five stations on each day are plotted in Fig. 9. It can be found that the multipath correction effect of the three different methods gradually degrades over the whole test period. XGB achieves the highest residual reduction rates for all four observables on the 25 test days. The reduction rates using XGB drop from 25.2%, 35.6%, 25.1% and 19.4% to 9.0%, 17.7%, 16.1% and 14.4% for P1, P2, L1 and L2 residuals, respectively. It means the multipath correction effect on DOY 273 is only half of that on DOY 249. A 5–7 days update rate seems to be a good trade-off between model validity and the workload of data processing. In this circumstance, it can still achieve 90% multipath correction effect of the daily updated model. SF performs similarly to XGB on the first day, but its performance rapidly drops on the subsequent three days and then decreases at a linear pace. That is mainly because the effectiveness of the SF model heavily depends on the accurate

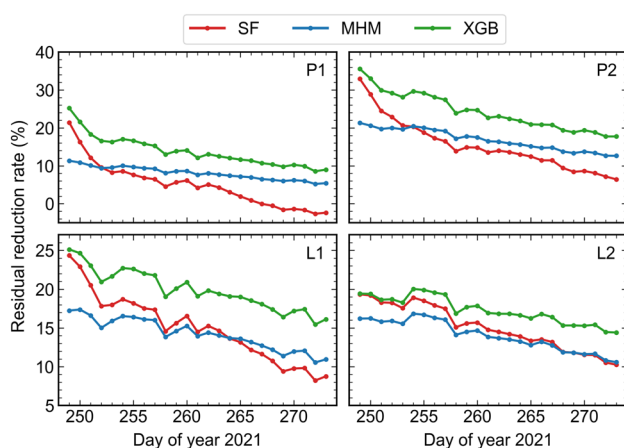


Fig. 9 Comparison of validity periods for different multipath models. Data from DOY 244–248 are used to set up the multipath models, which are later applied for multipath mitigation on DOY 249–273. The residual reduction rate on each day is the mean value of all five stations

orbit repeat time for each satellite on each day and any deviations between the computed and real orbit repeat time will impact the model performance. The MHM model performance is more stable, with the reduction rates dropping by 5.9%, 8.7%, 6.3% and 5.6% over the test periods for P1, P2, L1 and L2, respectively. It confirms that MHM model mainly captures the lower frequency multipath signals as they are more stable over time.

Positioning improvement

We further applied the three different multipath models for kinematic relative positioning. The model performance was evaluated regarding the positioning precision improvement compared to the solutions without correction. The daily static coordinates were used as the benchmark for calculation of positioning RMS. Note that multipath correction was not applied for static solutions as the impact of multipath on daily static positioning could be neglected. We finally obtained 125 time series (at five stations over 25 days) for each type of solution, i.e., raw (without correction), corrected with SF, MHM and XGB.

Figure 10 depicts the displacements for four different solutions at station CUCC on DOY 273. The raw solution contains many variations induced by multipath spanning from tens of seconds to half an hour, which are evident in all three coordinate components. These variations are effectively mitigated by applying the multipath models of SF, MHM and XGB. The RMS of the solution corrected by XGB is 1.4 mm, 1.9 mm and 4.4 mm for east, north and up components, respectively, which are equal to those of SF. It is interesting that the MHM model can reach comparable positioning precisions, especially considering its disadvantage to capture high-frequency multipath signals. The RMS values are only 0.1 mm, 0.1 mm and 0.2 mm larger than the other two models in east, north and up components, respectively. Usually, the high-frequency multipath occurs when a satellite is at low elevations. Such low-elevation observations are down-weighted during data processing. This can explain the reasonable positioning precision of MHM although it is deficient in high-frequency multipath modeling. The mean positioning precisions over all five stations and 25 days are listed in Table 3. Again, XGB and SF can achieve the highest precisions, which are 1.6 mm, 1.9 mm and 4.5 mm for east, north and up components, respectively. Compared to the raw solutions, the improvements are about 20.0%, 17.4% and 16.7% for the three components. Despite XGB achieving approximately 0.5% higher residual reduction rate for carrier phase compared to SF, this advantage is not reflected in the positioning precision statistics due to the weak multipath environment in which the stations are located. The performance of MHM is a bit worse compared to XGB and SF, but it can still reach 15.0%, 13.0%

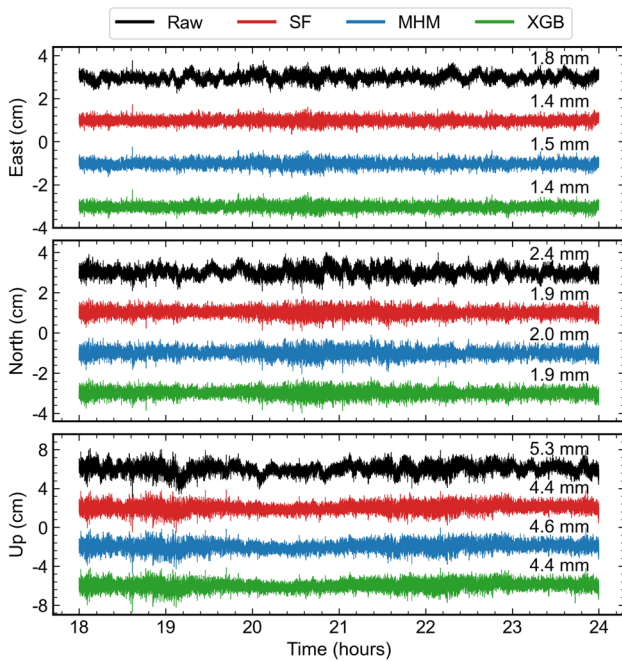


Fig. 10 1 Hz kinematic positioning results at station CUCC on DOY 273 with multipath mitigated with different methods. The raw positioning result and those corrected with SF, MHM and XGB are shown in black, red, blue and green curves, respectively. The individual curves are shifted along the y-axis to avoid overlapping. RMS values of displacements are denoted above each curve. Only the last 6 h displacements are displayed to show the detailed positioning errors induced by multipath

Table 3 Mean RMS of 1 Hz displacements in east, north and up components for four types of solutions over all five stations and 25 days

Method	Kinematic positioning precision (mm)		
	East	North	Up
Raw	2.0	2.3	5.4
Sidereal	1.6	1.9	4.5
MHM	1.7	2.0	4.7
XGB	1.6	1.9	4.5

and 13.0% precision improvements for east, north and up components, respectively.

Multipath mitigation for 30 s sampling data

In the last section, we have demonstrated the multipath mitigation performance of the XGB model using 1 s GPS data. However, 30 s is the more common sampling rate for most geodetic stations, such as the IGS network. Hence, we further validate the XGB model using GPS data of 30 s interval.

We reprocessed the data at 30 s sampling rate for all five stations and utilized the 30 s sampling residuals from 5 days before each target day to set up the multipath models for SF, MHM and XGB, respectively. Then, the residuals of P1, P2,

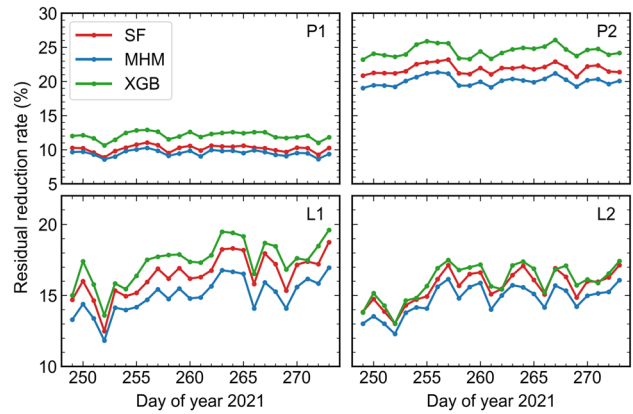


Fig. 11 Residual reduction rates for 30 s sampling data using different multipath mitigation methods. The residual reduction rate on each day is the mean value of all five stations

Table 4 Mean residual reduction rates for 30 s data over all five stations and 25 days

Model	Residual reduction rate (%)			
	P1	P2	L1	L2
SF	10.2	21.8	16.3	15.6
MHM	9.5	20.0	14.9	14.7
XGB	12.1	24.5	17.3	16.0

L1 and L2 are corrected with the corresponding models. The daily residual reduction rates are plotted in Fig. 11, and the mean values over 25 days are given in Table 4. We find that the reduction rates of XGB are the highest among the three different methods. The performance of XGB is almost constantly 1.9% and 2.6% higher than for SF and MHM for P1 residuals and 2.7% and 4.5% for P2. For carrier phase residuals, the reduction rates of XGB are about 1.0% and 2.4% higher than for SF and MHM for L1, and 0.4% and 1.3% for L2. This demonstrates the superiority of ML methods for multipath mitigation. In the circumstance of 30 s sampling rate, the error of the orbit repeat time calculation might be up to 15 s, which will degrade the SF model performance. For 30 s data, the frequency of multipath signals will not be higher than 60 s. Hence, the performance of the MHM model is closer to SF and XGB. But there will also be fewer data points within each grid cell, which might degrade the stability of the MHM model. The corresponding kinematic positioning results are listed in Table 5. It is found that XGB can achieve 0.1 mm higher precision in both north and up components than those of SF and MHM. The improvement compared to SF and MHM may not be evident because the data were collected in a weak multipath environment. Compared to the raw solutions, precision improvements of 15.0%, 13.0% and 11.3% can be achieved with the XGB model in east, north and up components, respectively.

Table 5 Mean RMS of 30 s displacements in east, north and up components for four types of solutions over all five stations and 25 days

Method	Kinematic positioning precision (mm)		
	East	North	Up
Raw	2.0	2.3	5.3
Sidereal	1.7	2.1	4.8
MHM	1.7	2.1	4.8
XGB	1.7	2.0	4.7

Multipath mitigation for low-cost devices

In the previous sections, we focused exclusively on geodetic GNSS stations operating within a weak multipath environment. To further demonstrate the applicability of our method, we applied it to a u-blox data set collected by Hohensinn et al. (2022) atop the HPV building of ETH Zurich. The data collection, spanning from DOY 104 to 109 in 2021, employed a u-blox ZED-F9P receiver alongside an ANN-MB antenna. Given the use of a low-cost patch antenna, significant multipath interference was anticipated. Additional data collection details can be found in Hohensinn et al. (2022). A geodetic station on the same rooftop was employed to form a short baseline. We processed the 1 Hz GPS data with the same strategies and constructed multipath models using SF, MHM and XGB, respectively. Note that for SF, the orbit repeat periods needed updating in this different time period. The residuals from the first five days were used to establish the multipath models, subsequently applied to DOY 109.

Figure 12 displays the results of residual reduction for satellite G03 on DOY 109. The carrier phase multipath is found to be approximately twice as large as that observed in the geodetic stations. Among the methods, XGB demonstrates the largest residual reduction rates for this satellite, reaching 50.7%, 51.9%, 61.9% and 54.1% for P1, P2, L1 and L2, respectively. The advantage of the XGB model is most evident around 19 h and 23 h, where multipath errors are more pronounced. Here, XGB evidently outperforms MHM and SF regarding multipath mitigation. The mean residual reduction rates for all satellites are shown in Table 6. XGB achieves about 3% and 15% higher residual reduction rates for carrier phase than SF and MHM, respectively. This improvement is also reflected in the kinematic positioning test, as depicted in Fig. 13. Compared to the raw solution, the positioning precision improves by 39.7%, 44.0% and 38.6% for east, north and up components, respectively, when employing XGB for multipath correction. The XGB-based solution surpasses SF by 0.2 mm and 0.5 mm in north and up components, respectively. Thus, XGB exhibits higher improvement in multipath mitigation for low-cost devices than for geodetic stations operating in weak multipath environments.

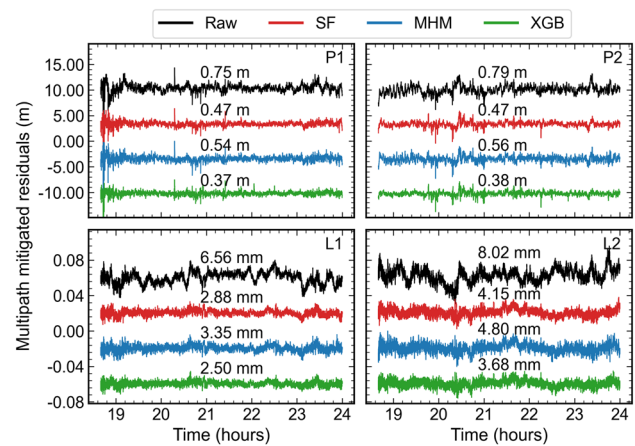


Fig. 12 Raw and multipath corrected residuals of satellite G03 from a u-blox data set on DOY 109. The individual curves are shifted along the y-axis to avoid overlapping. The RMS value is denoted above each curve

Table 6 Mean residual reduction rates for u-blox data on DOY 109, 2021

Model	Residual reduction rate (%)			
	P1	P2	L1	L2
SF	40.5	33.7	58.0	56.1
MHM	26.7	23.4	45.4	44.3
XGB	40.7	36.9	60.8	59.6

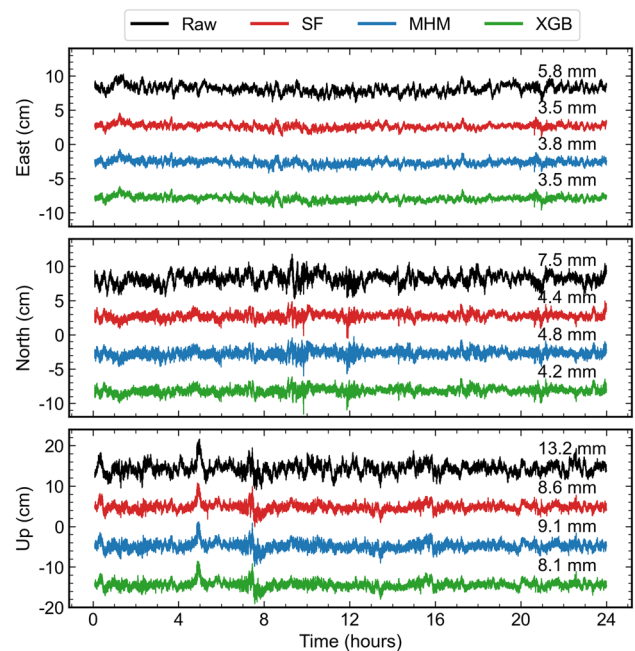


Fig. 13 1 Hz kinematic positioning results for a u-blox data set on DOY 109 with multipath corrected with different methods. The individual curves are shifted along the y-axis to avoid overlapping. RMS values of displacements are denoted above each curve

Conclusion

Multipath is the main unmodeled error in high-precision GNSS data processing. In this study, we proposed an ML-based multipath mitigation method. It takes azimuth and elevation as input features and outputs multipath corrections for pseudorange and carrier phase on both frequencies. Owing to its ability of spatial interpolation, it can outperform the conventional multipath mitigation methods. With 30 days of 1 Hz GPS data from five baselines on the rooftop of Curtin University, we validated the superiority of the ML-based multipath mitigation method. It was found that XGB with azimuth and elevation as input features could reach the best multipath mitigation effect. Adding calibrated SNR as an additional feature can only slightly improve the model performance for pseudorange but not for carrier phase. This phenomenon may be attributed to both the time lag between SNR variations and carrier phase multipath and the insufficient numeric precision of SNR measurements used in this study. We demonstrate that the XGB model can achieve 24.9%, 36.2%, 25.5% and 20.4% reduction rates for P1, P2, L1 and L2 residuals, respectively. Such performance is similar to SF but without the inconvenience of computing the orbit repeat period for each satellite. XGB can reach 14.0% and 5.8% more reduction rates than MHM for pseudorange and carrier phase residuals, respectively. After applying the XGB model, kinematic positioning precisions of 1.6 mm, 1.9 mm and 4.5 mm can be achieved in east, north and up components, respectively, which are 20.0%, 17.4% and 16.7% improvements compared to the raw solutions. The effectiveness of the XGB model for 30 s sampling data was also evaluated and compared to that of SF and MHM. It confirms that the advantage of spatial interpolation holds for low-sampling data. Residual reduction rates of 12.1%, 24.5%, 17.3% and 16.0% can be reached for P1, P2, L1 and L2, respectively, which are better than for SF and MHM. The advantage of the XGB model over SF and MHM becomes more pronounced when applied to a u-blox data set, where multipath is more severe due to the utilization of a patch antenna during data collection.

Although we only demonstrated the ML-based multipath mitigation using baseline data in this study, it is also valid for PPP multipath modeling and mitigation according to our preliminary internal tests. Since the ML-based model has the merit of ease of use, it is also promising for real-time applications, such as structural health monitoring. Besides, the ML-based model can be extended to include additional input features, such as environmental information and SNR measurements with higher numerical precision. However, further research is needed to better understand and refine the application of SNR for carrier phase multipath modeling. This might be helpful to further

improve the model, especially in long-term performance. Finally, more sophisticated ML algorithms are worth further investigation. As demonstrated in this study, basic tree-based ML algorithms can perform well for multipath modeling. More powerful algorithms, such as deep learning and reinforcement learning, can be further examined for multipath mitigation in future studies.

Acknowledgements The authors would like to thank Curtin GNSS-SPAN Group for the access to the high-rate GNSS data, Amir Allahviridi-Zadeh for providing the station photos, and Dr. Hohensinn for providing the u-blox data. The authors also would like to acknowledge the editor and two anonymous reviewers for their constructive comments.

Authors' contributions YP designed the study, analyzed the data and wrote the paper. GM and BS supervised the study and revised the manuscript. All authors reviewed the manuscript and approved it for publication.

Funding Open access funding provided by Swiss Federal Institute of Technology Zurich.

Availability of data and materials The high-rate GNSS data used in this study are available at <http://saegnss2.curtin.edu.au/ldc/>.

Declarations

Competing interests The authors declare no competing interests.

Open Access This article is licensed under a Creative Commons Attribution 4.0 International License, which permits use, sharing, adaptation, distribution and reproduction in any medium or format, as long as you give appropriate credit to the original author(s) and the source, provide a link to the Creative Commons licence, and indicate if changes were made. The images or other third party material in this article are included in the article's Creative Commons licence, unless indicated otherwise in a credit line to the material. If material is not included in the article's Creative Commons licence and your intended use is not permitted by statutory regulation or exceeds the permitted use, you will need to obtain permission directly from the copyright holder. To view a copy of this licence, visit <http://creativecommons.org/licenses/by/4.0/>.

References

- Agnew DC, Larson KM (2006) Finding the repeat times of the GPS constellation. *GPS Solut* 11(1):71–76. <https://doi.org/10.1007/s10291-006-0038-4>
- Atkins C, Ziebart M (2015) Effectiveness of observation-domain sidereal filtering for GPS precise point positioning. *GPS Solut* 20(1):111–122. <https://doi.org/10.1007/s10291-015-0473-1>
- Beroza GC, Segou M, Mostafa MS (2021) Machine learning and earthquake forecasting—next steps. *Nat Commun* 12(1):1–3. <https://doi.org/10.1038/s41467-021-24952-6>
- Bilich A, Larson KM, Axelrad P (2008) Modeling GPS phase multipath with SNR: case study from the Salar de Uyuni, Bolivia. *J Geophys Res*. <https://doi.org/10.1029/2007jb005194>
- Bilich A, Axelrad P, Larson KM (2007) Scientific utility of the signal-to-noise ratio (SNR) reported by geodetic GPS receivers. In:

- Proceedings of ION GNSS 2007, Institute of Navigation, Fort Worth, Texas, USA, September 25–28, 1999–2010
- Bock Y, Prawirodirdjo L, Melbourne TI (2004) Detection of arbitrarily large dynamic ground motions with a dense high-rate GPS network. *Geophys Res Lett*. <https://doi.org/10.1029/2003GL019150>
- Breiman L (2001) Random forests. *Mach Learn* 45(1):5–32. <https://doi.org/10.1023/A:1010933404324>
- Chen T, Guestrin C (2016). XGBoost: a scalable tree boosting system. In: Proceedings of the 22nd ACM SIGKDD international conference on knowledge discovery and data mining, pp 785–794. <https://doi.org/10.1145/2939672.2939785>
- Choi K, Bilich A, Larson KM, Axelrad P (2004) Modified sidereal filtering: implications for high-rate GPS positioning. *Geophys Res Lett*. <https://doi.org/10.1029/2004gl021621>
- Choy S, Bisnath S, Rizos C (2016) Uncovering common misconceptions in GNSS Precise Point Positioning and its future prospect. *GPS Solut* 21(1):13–22. <https://doi.org/10.1007/s10291-016-0545-x>
- Dong D, Wang M, Chen W, Zeng Z, Song L, Zhang Q, Cai M, Cheng Y, Lv J (2015) Mitigation of multipath effect in GNSS short baseline positioning by the multipath hemispherical map. *J Geod* 90(3):255–262. <https://doi.org/10.1007/s00190-015-0870-9>
- Geng J, Pan Y, Li X, Guo J, Liu J, Chen X, Zhang Y (2018) Noise characteristics of high-rate multi-GNSS for subdaily crustal deformation monitoring. *J Geophys Res Solid Earth* 123(2):1987–2002. <https://doi.org/10.1002/2018jb015527>
- Genrich JF, Bock Y (1992) Rapid resolution of crustal motion at short ranges with the global positioning system. *J Geophys Res Solid Earth* 97(B3):3261–3269. <https://doi.org/10.1029/91JB02997>
- Hilla S, Cline M (2004) Evaluating pseudorange multipath effects at stations in the National CORS Network. *GPS Solut* 7:253–267. <https://doi.org/10.1007/s10291-003-0073-3>
- Hohensinn R, Stauffer R, Glaner MF, HerreraPinzón ID, Vuadens E, Rossi Y, Clinton J, Rothacher M (2022) Low-cost GNSS and real-time PPP: assessing the precision of the u-blox ZED-F9P for kinematic monitoring applications. *Remote Sens* 14(20):5100. <https://doi.org/10.3390/rs14205100>
- Hsu LT (2017) GNSS multipath detection using a machine learning approach. In: 2017 IEEE 20th international conference on intelligent transportation systems (ITSC), pp 1–6
- Larson KM (2009) GPS seismology. *J Geod* 83(3–4):227–233. <https://doi.org/10.1007/s00190-008-0233-x>
- Li J, Heap AD, Potter A, Daniell JJ (2011) Application of machine learning methods to spatial interpolation of environmental variables. *Environ Model Softw* 26(12):1647–1659. <https://doi.org/10.1016/j.envsoft.2011.07.004>
- Lyu Z, Gao Y (2020a) A new method for non-line-of-sight GNSS signal detection for positioning accuracy improvement in Urban environments. In: Proceedings of ION ITM 2020, Institute of Navigation, September 21–25, 2972–2988. <https://doi.org/10.33012/2020.17662>
- Lyu Z, Gao Y (2020b) An SVM based weight scheme for improving kinematic GNSS positioning accuracy with low-cost GNSS receiver in urban environments. *Sensors* 20(24):7265. <https://doi.org/10.3390/s20247265>
- Park KD, Nerem RS, Schenewerk MS, Davis JL (2004) Site-specific multipath characteristics of global IGS and CORS GPS sites. *J Geod* 77(12):799–803. <https://doi.org/10.1007/s00190-003-0359-9>
- Reischung P, Altamimi Z, Ray J, Garayt B (2016) The IGS contribution to ITRF2014. *J Geod* 90(7):611–630. <https://doi.org/10.1007/s00190-016-0897-6>
- Satirapod C, Rizos C (2005) Multipath mitigation by wavelet analysis for GPS base station applications. *Surv Rev* 38(295):2–10. <https://doi.org/10.1179/003962605791521699>
- Strode PR, Groves PD (2016) GNSS multipath detection using three-frequency signal-to-noise measurements. *GPS Solut* 20:399–412. <https://doi.org/10.1007/s10291-015-0449-1>
- Su M, Yang Y, Qiao L, Teng X, Song H (2021) Enhanced multipath mitigation method based on multi-resolution CNR model and adaptive statistical test strategy for real-time kinematic PPP. *Adv Space Res* 67(2):868–882. <https://doi.org/10.1016/j.asr.2020.10.035>
- Suzuki T, Kusama K, Amano Y (2020) NLOS multipath detection using convolutional neural network. In: Proceedings of ION ITM 2020, Institute of Navigation, September 21–25, 2989–3000. <https://doi.org/10.33012/2020.17663>
- Takasu T (2009) RTKLIB: open source program package for RTK-GPS. In: Proceedings of the FOSS4G
- Tao Y, Liu C, Chen T, Zhao X, Liu C, Hu H, Zhou T, Xin H, Neagu A (2021a) Real-time multipath mitigation in multi-GNSS short baseline positioning via CNN-LSTM method. *Math Probl Eng* 2021:1–12. <https://doi.org/10.1155/2021/6573230>
- Tao Y, Liu C, Liu C, Zhao X, Hu H, Xin H (2021b) Joint time-frequency mask and convolutional neural network for real-time separation of multipath in GNSS deformation monitoring. *GPS Solut*. <https://doi.org/10.1007/s10291-020-01074-y>
- Wang Z, Chen W, Dong D, Wang M, Cai M, Yu C, Zheng Z, Liu M (2019) Multipath mitigation based on trend surface analysis applied to dual-antenna receiver with common clock. *GPS Solut*. <https://doi.org/10.1007/s10291-019-0897-0>
- Ye S, Chen D, Liu Y, Jiang P, Tang W, Xia P (2014) Carrier phase multipath mitigation for BeiDou navigation satellite system. *GPS Solut* 19(4):545–557. <https://doi.org/10.1007/s10291-014-0409-1>
- Zhang Z, Li B, Gao Y, Shen Y (2019) Real-time carrier phase multipath detection based on dual-frequency C/N0 data. *GPS Solut* 23:1–13. <https://doi.org/10.1007/s10291-018-0799-6>
- Zheng K, Zhang X, Li P, Li X, Ge M, Guo F, Sang J, Schuh H (2019) Multipath extraction and mitigation for high-rate multi-GNSS precise point positioning. *J Geod* 93(10):2037–2051. <https://doi.org/10.1007/s00190-019-01300-7>
- Zhong P, Ding X, Yuan L, Xu Y, Kwok K, Chen Y (2010) Sidereal filtering based on single differences for mitigating GPS multipath effects on short baselines. *J Geod* 84(2):145–158. <https://doi.org/10.1007/s00190-009-0352-z>

Publisher's Note Springer Nature remains neutral with regard to jurisdictional claims in published maps and institutional affiliations.



Yuanxin Pan is currently a Ph.D. candidate at ETH Zurich. He received his master's degree from GNSS Research Center, Wuhan University in 2021. His current research interest is application of machine learning for GNSS data processing.



Gregor Möller is an Assistant Professor at TU Wien with a research focus on satellite navigation systems and their integration with other observation techniques for precise orbit determination, positioning, and environmental monitoring. Gregor earned a Dr.techn. degree in Engineering Sciences from TU Wien, served as a NASA postdoctoral fellow from 2018 to 2019 and then a senior scientist at ETH Zurich until his current appointment in 2023.



Benedikt Soja is an Assistant Professor of Space Geodesy at ETH Zurich. He obtained his Ph.D. from TU Wien in 2016 and then became a fellow of the NASA Postdoctoral Program at the Jet Propulsion Laboratory, California. His research focuses on the application of machine learning in geodesy.